Micropositioning of 2DOF Piezocantilever: LKF Compensation of Parasitic Disturbances

J. Escareno[1], J. Abadie[2], E. Piat[2] and M. Rakotondrabe[2]

***Abstract*— This paper presents a new control method devoted to improve the performances of 2-DOF piezoelectric actuator for precise positioning tasks. The piezoelectric actuator exhibits strong cross-couplings between its two axes and strong hysteresis and creep nonlinearities. These unwanted phenomena undeniably compromised therefore the final precision of the targeted tasks (micromanipulation) and should be conveniently accounted during the controller synthesis. In this paper, we proposed a combination of the discrete linear Kalman filtering with a closed-loop scheme to suppress the effects of the couplings and of the nonlinearities. The suggested method permits to improve the performances of the piezoelectric actuator without specific and detailed characterization and knowledges on the hysteresis and on the creep models. Extensive experiments were carried out with complex desired trajectories and demonstrate the efficiency of the novel approach.**

***Index Terms*— Piezoelectric Cantilever, linear Kalman filter, 2-DOF Micro-positioning, disturbance Estimation/Compensation**

I. Introduction

These last years, the advance of microrobotics has increasingly enhanced different applications. Particularly, in micromanipulation application, technologies based on piezoelectric actuators represent a wide spectrum ranging from walking actuators to multi-DOF positioning systems to pick-and-place of micro-sized objects. The advantageous performances profile provided by piezoelectrical actuators (PEAs), which offer high bandwidth and high resolution, is degraded by static and dynamic disturbances (hysteresis and creep). Hysteretic behavior of PEAs is dependent on both current and past inputs. Hysteresis arises either in static regime (slow time-varying inputs) or dynamic regime (fast time-varying). Furthermore multi-DOF micropositioning applications bring unwanted cross-couplings effects either for sequenced or simultaneous motions. Robust control schemes are able to mitigate such adverse nonlinear phenomena.

The control of PEAs has been addressed using feedforward and feedback control approaches, or a combination of both. Feedforward-based schemes rely on the accuracy of the PEA's model so that its inverse can compensate hysteresis allowing that actual position reaches desired displacement. In feedforward control of piezoelectric actuators, several approaches are available to model and then to compensate for the hysteresis: the Preisach [1] [2] [3], the Prandtl-Ishlinskii [4] [5] [6] [7] and the Bouc-Wen approaches [8] [9]. In the two formers, a complex hysteresis is modeled by the sum of many basic hysteresis (hysterons). Both approaches can be very accurate with the use of a high number of elementary hysteresis, which represents a computational burden implementation. Alternatively, the Bouc-Wen model of hysteresis, has an interesting simplicity and is able to represent a large class of hysteresis. Although the low cost and the high packageability (no sensors required) of the used feedforward control approaches, their main limitation is the lack of robustness face to model uncertainties and to external disturbances.

Likewise, feedback control has been utilized to deal with the motion control of PEAs. In this case, the controller's performances will be as good as the quality of the measurements and/or the estimation of the system's states. Two control applicative categories might be distinguished based on the operational regime:

- *Low-frequency operations*
  In this regime, hysteresis, creep and couplings (multi-DOF PEAs) are considered as a constant disturbance introducing a static error. Thus, classical PID or event intelligent adaptive schemes can fullfil the control objective [10] [11].
- *High-frequency operations*
  The aforementioned parasitic disturbances become dynamic. Therefore, robust control schemes are required to overcome significant uncertainties. Recent works encompass sliding-mode control (SMC), SMC+adaptive and H_∞ schemes. Such controllers are able to reject the effect of the aforementioned disturbances [12] [13] [14] [15] [16].

State observers, either deterministic or stochastic, represent an interesting alternative for both operation profiles, not only to estimate missing states (e.g. velocity) and/or to improve state(s) measurement(s) (e.g. filtering [17]) but also to estimate unknown inputs (1DOF unknown input observers [18], [19])

In the present paper is addressed a multi-DOF micropositioning application. Simultaneous motion resulting from the commanded trajectories generates nonlinear dynamic disturbances (hysteresis, creep and couplings) deteriorating significantly the motion objective. There-

[1]J. Escareno is with the Polytechnic Institute of Advanced Sciences, 7-9 rue M. Grandcoing, 94200 Ivry-sur-Seine, France
[2] AS2M department, FEMTO-ST Institute, UFC-CNRS-ENSMM-UTBM, Besançon, FRANCE

fore, it is proposed and implemented in real-time an estimation strategy based on the linear Kalman filter (LKF) to estimate the such parasitic disturbance. It is also presented a simple-to-implement closed-loop scheme, whose successful application (i.e. canceling out undesired/parasitic effects) validates the effectiveness of the disturbance estimation algorithm.

Experimental result are provided to evaluate the performance of the piezocantilever while tracking a circular trajectory.

The paper is organized as follows: the description and model of the piezocantilever is presented in section-II. In section-III the characteristics of the experimental setup are described. In section-IV is described the LKF-based estimation algorithm as well as the closed-loop compensation scheme. Experimental results are presented in section-V. Finally, the conclusions and perspectives are given in section-VI.

II. Modeling of the Piezocantilever

The actual paper considers as reference model for the piezocantilever the Bouc-Wen model of hysteresis, which corresponds to a cascade structure featuring a static hysteresis model plus a second order linear dynamic system (see Fig. 1). Such model stands out for its simplicity reagarding computation and implementation. Another aspect, is the compatibility of the the Bouc-Wen model for controllers synthesis [8] [9].

The nonlinear equations which model the behavior of the multi-DOFs piezocantilever are written as

$$\begin{cases} a_i\ddot{\delta}_i + b_i\dot{\delta}_i + \delta_i = d_{pi}U_i - h_i \\ \dot{h}_i = d_{pi}A_{bwi}\dot{U}_i - B_{bwi}\left|\dot{U}_i\right| h_i - C_{bwi}\dot{U}_i\,|h_i| \end{cases} \tag{1}$$

where $i \in \{y, z\}$, A_{bwi}, B_{bwi} and C_{bwi} are coefficients determining the hysteresis shape and amplitude and d_pi is a positive coefficient that defines the magnitude deflection, while h_i represents the hysteresis internal state.

During multi-DOF micropositioning operation, novel disturbances arise besides the hysteresis and creep. The motion along every axis, $y - z$ in this case, generates reciprocal input-dependent dynamic couplings degrading the overall positioning performance (see Fig. 8). Such couplings effects increase during simultaneous operations which correspond for instance to trajectory tracking tasks. For this reason, the previous nonlinear model can

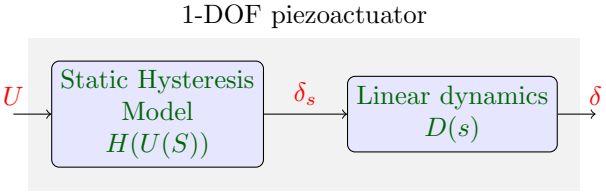

Fig. 1: Hammerstein Model of a 1-DOF Piezocantilever

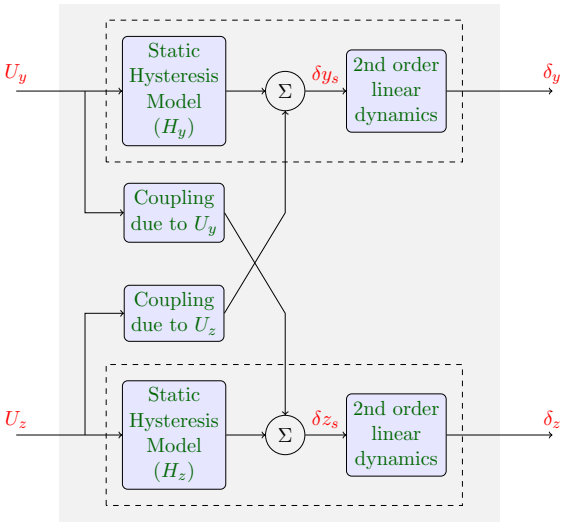

Fig. 2: Block scheme of coupling's structure

be rewritten to encompass not only creep but also the aforementioned couplings [4].

$$\begin{cases} a_i\ddot{\delta}_i + b_i\dot{\delta}_i + \delta_i = d_{pi}U_i + \Theta_i \\ \text{with } \Theta_i = -h_i + \mathcal{C}_{di} + \mathcal{C}_{ri} \end{cases} \tag{2}$$

where $\mathcal{C}_{di}$ and $\mathcal{C}_{ri}$ stand for the coupling and creep, respectively. The couplings structure is illustrated on Fig.2.

III. Experimental Setup Description

The experimental platform features a multi-DOF piezocantilever (y-z axes). This actuator is designed with 36 piezo-electric layers to work at low input voltage. The total dimensions of the active part are 25x1x1 mm^3. This cantilever is controlled by two inputs U_y and U_z that are varying in the range of $\pm$20 volts. The first extremity of the cantilever is clamped while the other moves within the 2D y-z plane based on the input U_i with $i \in \{y, z\}$ (see Fig. 3).

The cantilever displacement in the 2D y-z plane is given by the vector $\vec{\delta}$. The measurement $\vec{L}_m$ of $\vec{\delta}$ is performed using two external confocal sensors orthogonally arranged that are pointing at the tip of the piezocantilever, along the y and z axes (see Fig. 3). Each confocal sensor provides a measurement of δ_i, with $i \in \{y, z\}$.

The displacement measurement is acquired by a dSpace DS1005 acquisition system. The measurements performed by the confocal sensors will be considered as the real position and features a noise ν_i due to the electronic conditioning of the position signals. i.e.

$$\delta_i + \nu_i = \begin{pmatrix} \delta_y + \nu_y \\ \delta_z + \nu_z \end{pmatrix} \tag{3}$$

It is assumed that $\nu_y = \nu_z$.

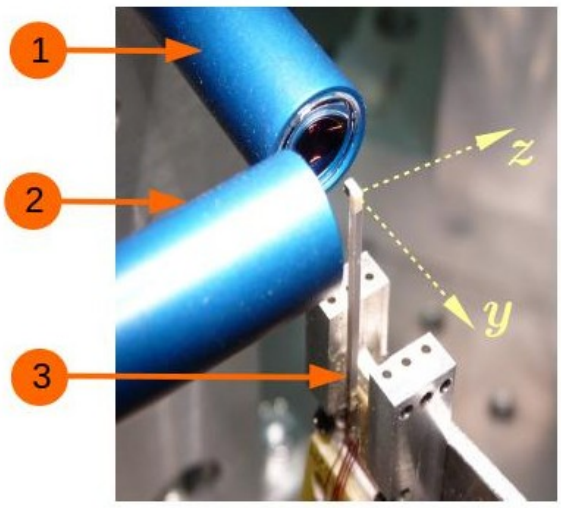

Fig. 3: Experimental setup: 1) y-axis confocal sensor, 2) z-axis confocal sensor and 3) Piezoelectric cantilever

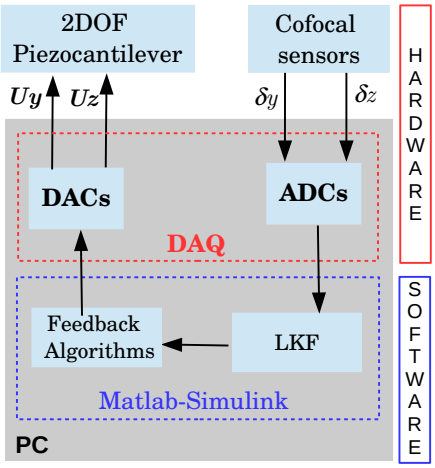

Fig. 4: Experimental architecture

A. Model Identification

The parameters corresponding to the dynamics (Equ.1) of the piezocantilever have been identified using the ARMAX approach (Autoregressive-moving-average model with exogenous inputs) with an experimental 10 Volts step response applied to the piezocantilever (see Tab. I). For instance, Fig. 5 illustrates the identification process for the $y-$axis and its coupling to the $z-$axis. Such values were used in a prior simulation study so that we can evaluate the performance of the proposed control law and they will be used during the estimation stage described in the further sections. The parameters shaping the hysteresis have been obtained via a least-square algorithm implemented in Matlab and using experimental data from the piezocantilever.

Parameter	value	Parameter	value
a_y	4.4209×10^{-9}	a_z	3.5125×10^{-9}
b_y	$3.7378\times^{-6}$	b_z	2.9062×10^{-5}
d_{p_y}	5.13	d_{p_z}	3.702

TABLE I: Dynamic parameters of the piezocantilever.

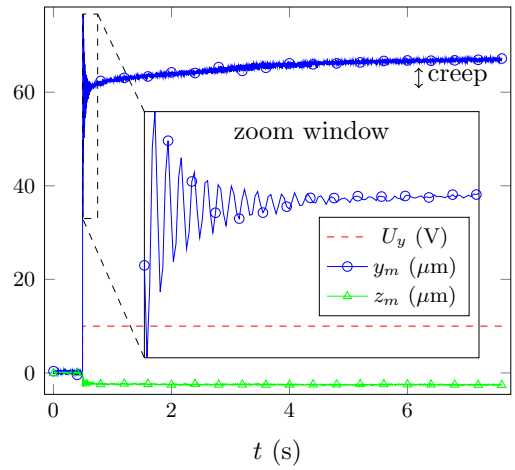

Fig. 5: piezocantilever step response to a 10 V step input U_y ($U_z = 0$)

IV. Coupling, hysteresis and creep compensation principle

A discrete linear Kalman filter (LKF) is designed and implemented in real-time regarding the estimation of the disturbances arising during a two-dimensional micro-positioning task of the piezocantilever in the plan y-z. The Linear Kalman Filter (LKF) is derived from a continuous system

$$\begin{cases} \dot{x}(t) &= Ax(t) + Bu(t) + \mathcal{M}\omega(t) & \rightarrow \text{process} \\ y(t) &= Cx(t) + \nu(t) & \rightarrow \text{sensor(s)} \end{cases} \tag{4}$$

that considers the following hypothesis:

H1. The pair AC verifies the controllability property

H2. The signals ω and ν stand for a white Gaussian random process with zero-mean ($E[\omega(t)] = 0$) and $E[\nu(t)] = 0$)) with constant power spectral density (PSD) $W(t)$ and $V(t)$ defining respectively:

- The process covariance matrix

$$Q = E\left[\omega(t)\omega(t+\tau)^T\right] = W\Delta(\tau) \tag{5}$$

- The sensor covariance matrix

$$R = E\left[\nu(t)\nu(t+\tau)^T\right] = V\Delta(\tau) \tag{6}$$

It is also assumed that both stochastic processes are not correlated, i.e.

$$E\left[\omega(t)\nu(t)^T\right] = 0 \tag{7}$$

A. LKF-based Estimation Strategy

Let us recall the piezocantilever model given by Equ. 2

$$a_i\ddot{\delta}_i + b_i\dot{\delta}_i + \delta_i = d_{pi}U_i + \Theta_i \text{ with } i \in \{y, z\} \quad (8)$$

This model corresponds to two scalar disturbed systems defining the motion behavior along y and z axes (see Fig. 6). This model may be rewritten into the space-state representation

$$\begin{aligned} \dot{x} &= Ax + Bu + Pd \\ y &= Cx \end{aligned} \quad (9)$$

having as a state vector $x = (\delta_i, \dot{\delta}_i)^T$. The positions provided by the confocal chromatic sensors are the outputs $y = \delta_i$ and $d = \Theta_i$ corresponds to the dual-axis disturbance. The matrices of the system (Equ. 9) are given by:

$$A = \begin{pmatrix} 0 & 1 \\ -\frac{1}{a_i} & -\frac{b_i}{a_i} \end{pmatrix} B = \begin{pmatrix} 0 \\ \frac{d_{pi}}{a_i} \end{pmatrix} P = \begin{pmatrix} 0 \\ \frac{1}{a_i} \end{pmatrix} C = \begin{pmatrix} 1 & 0 \end{pmatrix} \quad (10)$$

It is assumed that no prior information about the disturbance is available. However, we consider that the disturbance has a slow time-varying dynamics that can be modeled by a random walk process

$$\dot{\Theta}_i = \omega \quad (11)$$

with $\omega(t)$ defined by **H2**. The latter assumption allows us to introduce an extended state-space vector:

$$x^e(t) = (\delta_i, \dot{\delta}_i, \Theta_i)^T \quad (12)$$

and its associated state-space model describing the dynamics is obtained from (Equ. 11) in which the unknown input disturbance $\Theta^x(t)$ is incorporated in the transition matrix:

$$\begin{aligned} \dot{x}^e(t) &= \mathcal{A}x^e(t) + \mathcal{B}u + \mathcal{M}\omega \quad (13) \\ y(t) &= \mathcal{C}x^e(t) + \nu \quad (14) \end{aligned}$$

with

$$\mathcal{A} = \begin{pmatrix} 0 & 1 & 0 \\ -\frac{1}{a_i} & -\frac{b_i}{a_i} & \frac{1}{a_i} \\ 0 & 0 & 0 \end{pmatrix} \quad \mathcal{B} = \begin{pmatrix} 0 \\ \frac{d_{pi}}{a_i} \\ 0 \end{pmatrix} \quad (15)$$

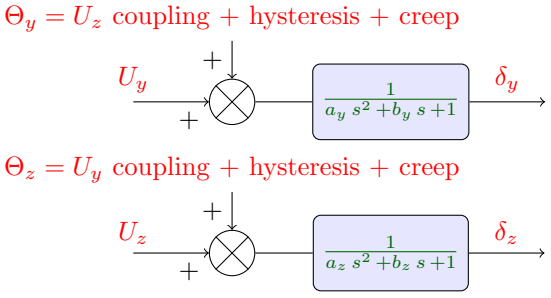

Fig. 6: Simplified disturbed model

$$\mathcal{M} = \begin{pmatrix} 0 \\ 0 \\ 1 \end{pmatrix} \quad \mathcal{C} = \begin{pmatrix} 1 & 0 & 0 \end{pmatrix} \quad (16)$$

The continuous-time model (Equ. 13) can be discretized with sampling time T_s. Assuming zero-order hold (zoh) of the input yields

$$\begin{aligned} x_k^e &= \mathcal{A}_k x_k^e + \mathcal{B}_k u_k + \omega_k \quad (17) \\ y_k &= \mathcal{C}_k x_k^e + \nu_k \quad (18) \end{aligned}$$

with

$$\begin{aligned} x_k^e &= (\delta_{i_k}, \dot{\delta}_{i_k}, \Theta_{i_k})^T \quad (19) \\ \mathcal{A}_k &= e^{\mathcal{A}T_s} \quad (20) \\ \mathcal{B}_k &= \left(\int_0^{T_s} e^{\mathcal{A}T_s}\right)\mathcal{B} \quad (21) \\ \omega_k &= (\omega_k^{\delta_i}, \omega_k^{\dot{\delta}_i}, \omega_k^{\Theta_i})^T \quad (22) \\ \nu_k &= \nu_k^{\delta_i} \quad (23) \end{aligned}$$

where ω_k and ν_k are discrete-time band-limited white gaussian random process with zero-mean characterizing uncertainties on the model (unmodeled dynamics or parametric uncertainties) and measurement (noisy sensors) equations, respectively.

The model uncertainties 3×3 covariance matrix Q is:

$$\begin{aligned} Q = E\left[\omega_k \omega_k^T\right] &= \int_0^{T_s} e^{\mathcal{A}t}\mathcal{M}W_{\dot{F}}\mathcal{M}^T e^{\mathcal{A}^T t}dt \\ &= W_{\dot{\Theta}_i}\int_0^{T_s} e^{\mathcal{A}t}\mathcal{M}\mathcal{M}^T e^{\mathcal{A}^T t}dt \\ &= W_{\dot{\Theta}_i}\,\eta(T_s) \end{aligned} \quad (24)$$

The latter equation shows that the covariance matrix Q is proportional to PSD $W_{\dot{\Theta}_i}$ and it can be shown with (Equ. 24) that the variance is

$$\sigma^2(\omega_k^{\Theta_i}) = Q_{33} = T_s W_{\dot{\Theta}_i} \quad (25)$$

The classical LKF is very attractive for experimental applications due to its simplicity and low computational demand. The algorithm that computes the estimate (including the disturbance Θ_i) of the state vector x_k^e is initialized as follows:

- The piezocantilever-based micro-positioning system is in the equilibrium state

$$x_{k_0}^e = (0, 0, 0)^T \quad (26)$$

- The initial covariance matrix P_0 is considered as

$$P_0 = \text{diag}\left[\sigma^2(\delta_{i_0}), \sigma^2(\dot{\delta}_{i_0}), \sigma^2(\Theta_{i_0})\right] \quad (27)$$

The corresponding LKF recursive algorithm features a

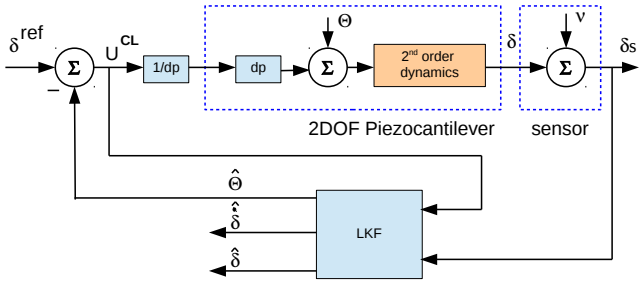

Fig. 7: Closed-loop architecture

prediction-estimation structure and is provided next

$$\texttt{Prediction stage}$$
$$\hat{x}_{est_k} = \mathcal{A}_k \hat{x}_{est_k} + \mathcal{B}_k u_k$$
$$P_{pred_k} = \mathcal{A}_k P_{est_k} \mathcal{A}_k^T + Q$$
$$K_k = P_{pred_k} \mathcal{C}_k^T \left(\mathcal{C}_k P_{pred_k} \mathcal{C}_k^T + R\right)^{-1}$$
$$\texttt{Estimation stage}$$
$$y_k = \text{measurement vector}$$
$$\hat{x}_{est_k} = \hat{x}_{pred_k} + K_k \left(y_k - \mathcal{C}_k \hat{x}_{pred_k}\right)$$
$$P_{est_k} = \left(I - K_k \mathcal{C}_k\right) P_{pred_k} \left(I - K_k \mathcal{C}_k\right)^T$$

where K_k denotes the Kalman filter gain, and I is the identity matrix. The estimated vector state generated by the LKF is the written:

$$\hat{x}_k^e = (\hat{\delta}_{i_k}, \hat{\dot{\delta}}_{i_k}, \hat{\Theta}_{i_k})^T \tag{28}$$

For the actual work it was considered

$$\hat{\Theta}_{i_k} = \mathcal{C}_d \hat{x}_k^e \tag{29}$$

with $\mathcal{C}_d = (0, 0, 1)^T$

B. LKF-based Disturbance Compensation

The feedback compensation input U_i incorporates the output of the discrete LKF that corresponds to the overall estimated disturbance $\hat{\Theta}_i$. The closed-loop architecture is depicted in Fig. 7. Assuming the knowledge of the disturbance, the goal consists in changing the natural equilibrium point provided by the second-order stable behavior of the actual piezoactuator. Let us rewrite the dynamics model Equ.8 as

$$\ddot{\delta}_i = \frac{d_{pi} U_i - b_i \dot{\delta}_i - \delta_i + \Theta_i}{a_i} \tag{30}$$

whose vectorial space-system is given

$$\begin{pmatrix} \dot{\delta}_{i_1} \\ \dot{\delta}_{i_2} \end{pmatrix} = \underbrace{\begin{pmatrix} 0 & 1 \\ -\frac{1}{a_i} & -\frac{b_i}{a_i} \end{pmatrix}}_{A \text{ :Hurwitz}} \begin{pmatrix} \delta_{i_1} \\ \delta_{i_2} \end{pmatrix} + \underbrace{\begin{pmatrix} 0 \\ \frac{d_{pi}}{a_i} \end{pmatrix}}_{B} U_i + \underbrace{\begin{pmatrix} 0 \\ \frac{1}{a_i} \end{pmatrix}}_{P} \Theta_i \tag{31}$$

with $i \in \{y, z\}$. From the latter, it is straightforward to deduce the required feedback input to counteract the disturbance and to perform a change of coordinates, i.e.

$$u = \frac{1}{d_{p_i}} (\delta_i^{ref} - \hat{\Theta}_i) \tag{32}$$

Parameter	Value
sampling time T_s	0.2×10^{-3} [sec]
PSD W_{Θ_i}	0.01
R_i	0.04

TABLE II: Experimental parameters

Also, the feedback input Equ.32 allows to rewrite the system Equ.33 as

$$\begin{pmatrix} \dot{\xi}_{i_1} \\ \dot{\delta}_{i_2} \end{pmatrix} = \underbrace{\begin{pmatrix} 0 & 1 \\ -\frac{1}{a_i} & -\frac{b_i}{a_i} \end{pmatrix}}_{(A+KB) \text{ :Hurwitz}} \begin{pmatrix} \xi_{i_1} \\ \delta_{i_2} \end{pmatrix} \tag{33}$$

where $\xi_{1_i} = \delta_{1_i} - \delta_{1_i}^{ref}$. Since the matrix $A + BK$ is Hurwitz the states ξ_{1_i} and δ_{2_i} converge exponentially to zero, which implies that $\delta_{1_i} \to \delta_{1_i}^{ref}$.

V. Experimental Results

Section IV has detailed the estimation strategy of the generalized disturbance (dual-axis hysteresis, couplings and creep), where as the experimental results obtained from real-time implementation of the LKF-based strategy are discussed in this section. Firstly, it is presented the open-loop performance of the system with a circular trajectory reference. Moreover, a simple and disturbance feedback is implemented to introduce the estimated disturbance. The latter demonstrates the effectiveness of the disturbance estimation of the estimation algorithms counteract its adverse effects.

Real-time experiments were carried out using Matlab-Simulink® which is linked to the dSPACE® DAQ[1] via ControlDesk®. Experimental parameters are listed on the table II.

A. Open-loop Behavior

During micro-positioning operations the piezocantilever's performance is significantly deteriorated mainly due to hysteresis and creep. Indeed, besides these adverse effects, multi-DOFs (2DOF in our case) tasks features internal dynamic couplings. The curves matrix depicted in Fig.8 picture such parasitic relationship. The worst case occurs during simultaneous motion positioning. The curves depicted on Fig.?? and Fig.?? show the open-loop behavior while tracking circular trajectory (radius=$30\mu m$)

$$\begin{aligned} \delta_y(t)^d &= 30 \sin(2\pi f t) \\ \delta_z(t)^d &= 30 \cos(2\pi f t) \end{aligned} \tag{34}$$

at frequencies of $0.1Hz$ and $1Hz$. It is observed in that the error is quite significant reaching 30%. As witnessed by open-loop experimental results, Fig. 9 and Fig. 10, the need of incorporating not only a feedback approach but also disturbance-tolerant controllers either robust or observer-based.

[1] I/O Acquisition card

B. Closed-loop Behavior: Hysteresis, Creep and Couplings Compensation Performance

In order to show the effectiveness of the LKF-based estimation strategy, the closed-loop scheme illustrated by Fig. 7 is used to reject dynamic dual-axis disturbances due to simultaneous 2D motion (circular trajectory reference). In general, experimental results depicted in Fig. 11 and Fig. 12a reveals that motion objective is fulfilled. Specifically, Fig. 11 shows that the $0.1Hz$-circular reference is successfully tracked having errors below 2% for both axes. The latter implies the effective estimation of the overall dual-axis disturbance containing hysteresis, creep and couplings. Likewise, Fig. 12a shows that the $1Hz$-circular reference is successfully tracked having, once again, errors below 2% for both axes. Hence, to the actual value the overall dual-axis disturbance containing hysteresis, creep and couplings is well estimated.

square to improve the presentation.

VI. Concluding Remarks

This paper dealt with the control of two degrees of freedom (2-DOF) piezoelectric actuator (PEA) devoted to micromanipulation tasks. Although the actuator exhibit interesting bandwidth and positioning resolution, it is typified by strong couplings between its two axes, and strong hysteresis and creep nonlinearities. These couplings and nonlinear phenomena finally compromise the overall performances of the tasks: loss of accuracy, stability compromised. In this paper, we proposed a new strategy to control 2-DOF PEAs for microrobotics tasks. This strategy is based on two steps : firstly, an estimation of the hysteresis, creep and axis coupling effects, considered as an unknown disturbance input, is done with a LKF using an extended state including this unknown input. The unknown dynamic of this disturbance is simply modeled by a random walk process (aka Wiener process). Secondly, this estimation is used in a feedback scheme to compensate for this disturbance. Extensive experiments were carried out and demonstrate the efficiency of the proposed approach of modeling and control for low frequency trajectory tracking despite the simplicity of the feedback used. More elaborated control architecture should be developed to deal with high-speed tracking. For future works, we are planning to merge the proposed strategy with an sliding-mode controller.

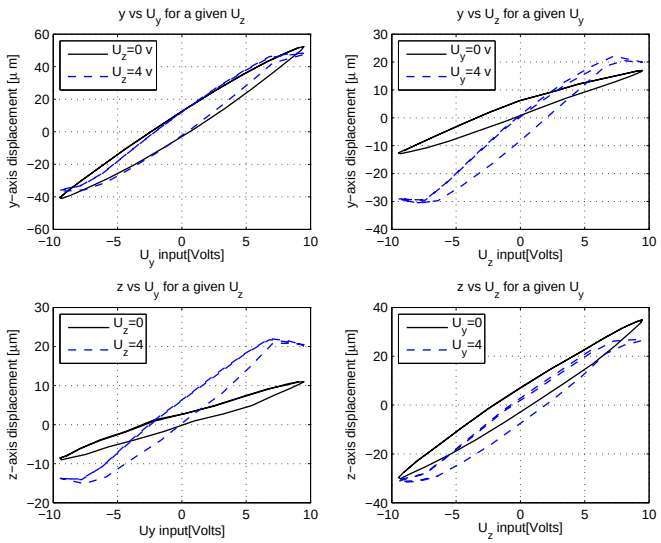

Fig. 8: Curves depicting the effect the dual-axis couplings

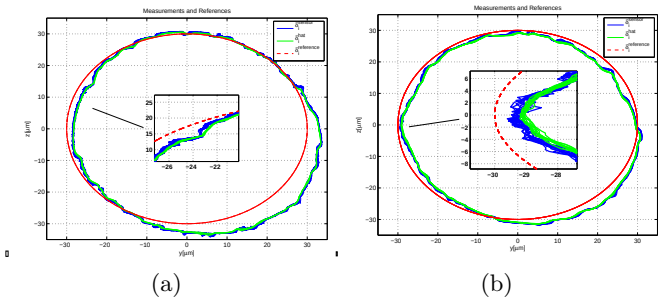

Fig. 9: Open-loop behavior using a circular trajectory reference (radius=$30\mu m$): (a) $f = 0.1Hz$ and (b) $f = 0.1Hz$

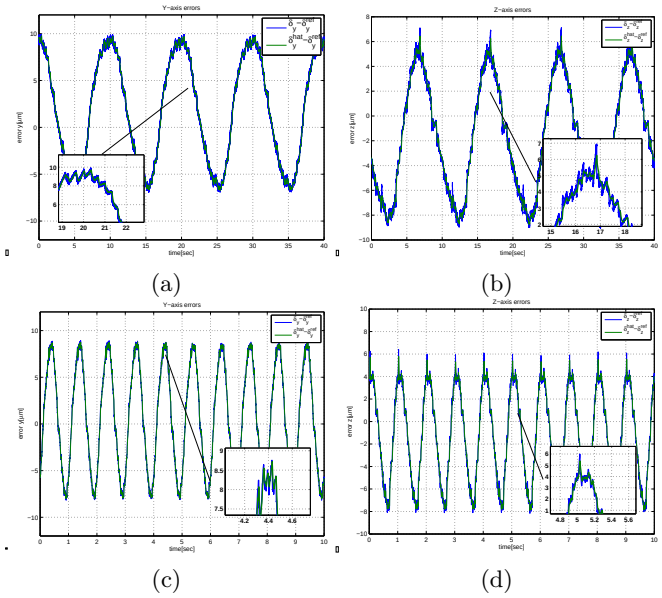

Fig. 10: Open-loop displacement errors resulting from the reference tracking: (a) e_y with $f = 0.1Hz$, (b) e_z with $f = 0.1Hz$, (c) e_y with $f = 1Hz$ and (d) e_z with $f = 1Hz$

Acknowledgement

This collaborative work has been supported by the Labex ACTION project (contract "ANR-11-LABX-01-01")

VII. Bibliography

References

[1] R.V. Iyer, X. Tan, and P.S. Krishnaprasad. Approximate inversion of the preisach hysteresis operator with application to control of smart actuators. *IEEE Transactions on Automatic Control*, 50(6), 2005.

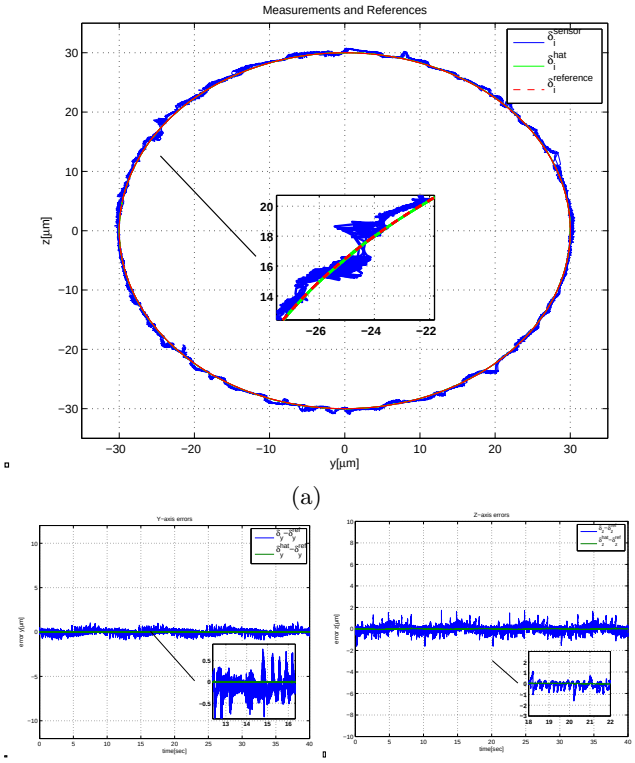

Fig. 11: Closed-loop performance @ 0.1Hz: (a) Circular trajectory tracking (b) y-axis errors (c) z-axis errors

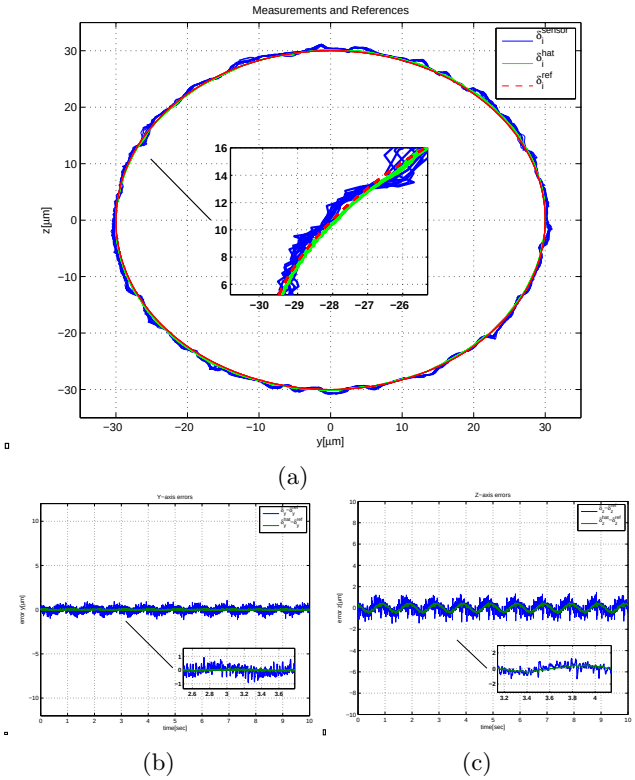

Fig. 12: Closed-loop performance @ 1Hz: (a) circular trajectory tracking (b) y-axis errors (c) z-axis errors

[2] G. Shed D. Croft and S. Devasia. Creep, hysteresis and vibration compensation for piezoactuators: atomic force microscopy application. *ASME Journal of Dynamic Systems, Measurement and Control*, 123(50), 1999.

[3] A. Dubra, J. Massa, and C.L. Paterson. Preisach classical and nonlinear modeling of hysteresis in piezoceramic deformable mirrors. *Optics Express*, 13(22), 2005.

[4] M. Rakotondrabe, C. Clevy, and P. Lutz. Complete open loop control of hysteretic, creeped, and oscillating piezoelectric cantilevers. *IEEE Transactions on Automation Science and Engineering*, 7(3):440–450, 2010.

[5] B. Mokaberi and A. A. G. Requicha. Compensation of scanner creep and hysteresis for afm nanomanipulation. *IEEE Transactions on Automation Science and Engineering*, 5(2), 2008.

[6] M. Rakotondrabe. Classical prandtl-ishlinskii modeling and inverse multiplicative structure to compensate hysteresis in piezoactuators. *American Control Conference*, 2012.

[7] M. Al Janaideh and P. Krejci. Inverse rate-dependent prandtl-ishlinskii model for feedforward compensation of hysteresis in a piezomicropositioning actuator. *IEEE/ASME Transactions on Mechatronics*, 18(5), 2013.

[8] Micky Rakotondrabe. Bouc-wen modeling and inverse multiplicative structure to compensate hysteresis nonlinearity in piezoelectric actuators. *IEEE Transactions on Automation Science and Engineering*, 8(2), 2011.

[9] Didace Habineza, Micky Rakotondrabe, and Yann Le Gorrec. Bouc-wen modeling and feedforward control of multivariable hysteresis in piezoelectric systems: Application to a 3-dof piezotube scanner. *IEEE Transactions on Control Systems Technology*, DOI.10.1109/TCST.2014.2386779., 2015.

[10] Faa-Jeng Lin, Hsin-Jang Shieh, Po-Kai Huang, and Li-Tao Teng. Adaptive control with hysteresis estimation and compensation using rfnn for piezo-actuator. *Ultrasonics, Ferroelectrics, and Frequency Control, IEEE Transactions on*, 53(9):1649–1661, Sept 2006.

[11] Faa-Jeng Lin, Hsin-Jang Shieh, and Po-Kai Huang. Adaptive wavelet neural network control with hysteresis estimation for piezo-positioning mechanism. *Neural Networks, IEEE Transactions on*, 17(2):432–444, March 2006.

[12] Yangmin Li and Qingsong Xu. Adaptive sliding mode control with perturbation estimation and pid sliding surface for motion tracking of a piezo-driven micromanipulator. *Control Systems Technology, IEEE Transactions on*, 18(4):798–810, July 2010.

[13] Xinkai Chen and T. Hisayama. Adaptive sliding-mode position control for piezo-actuated stage. *Industrial Electronics, IEEE Transactions on*, 55(11):3927–3934, Nov 2008.

[14] A. Sebastian, M. V. Salapaka, and J. P. Cleveland. Robust control approach to atomic force microscopy. *Conference on Decision and Control*, 2003.

[15] Sofiane Khadraoui, Micky Rakotondrabe, and Philippe Lutz. Combining h-inf approach and interval tools to design a low order and robust controller for systems with parametric uncertainties: application to piezoelectric actuators. *International Journal of Control*, 85(3), 2012.

[16] Juan Escareno. Backstepping-based robust-adaptive control of a nonlinear 2-dof piezoactuator. *Control Engineering Practice*, 41(57-71), 2015.

[17] M. Boudaoud, Y. Haddab, and Y. Le Gorrec. Modeling and optimal force control of a nonlinear electrostatic microgripper. *Mechatronics, IEEE/ASME Transactions on*, 18(3):1130–1139, June 2013.

[18] M. Rakotondrabe and P. Lutz. Force estimation in a piezoelectric cantilever using the inverse-dynamics-based uio technique. In *Robotics and Automation, 2009. ICRA '09. IEEE International Conference on*, pages 2205–2210, May 2009.

[19] E. Piat, J. Abadie, and S. Oster. Nanoforce estimation with kalman filtering applied to a force sensor based on diamagnetic levitation. In *Intelligent Robots and Systems (IROS), 2011 IEEE/RSJ International Conference on*, pages 39–44, Sept 2011.